

Aluminum Nanoarrays for Plasmon-Enhanced Light Harvesting

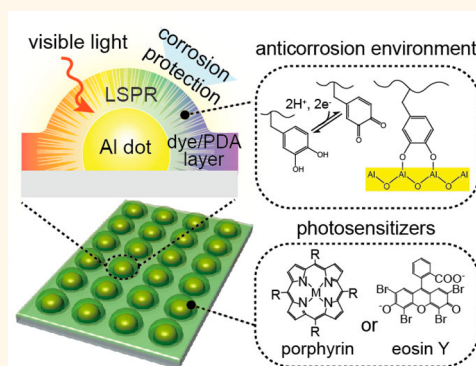
Minah Lee,[†] Jong Uk Kim,[†] Ki Joong Lee,[‡] SooHoon Ahn,[§] Yong-Beom Shin,^{*,‡,||} Jonghwa Shin,^{*,†} and Chan Beum Park^{*,†}

[†]Department of Materials Science and Engineering, Korea Advanced Institute of Science and Technology, 291 Daehak-ro, Daejeon 305-338, Republic of Korea,

[‡]Biomedical Translational Research Center, Korea Research Institute of Bioscience and Biotechnology, 125 Gwahak-ro, Daejeon 305-806, Republic of Korea,

[§]Department of Mechanical & Materials Engineering, Korea Institute of Nuclear Safety, and ^{||}Nanobiotechnology Major, Korea University of Science and Technology, 217 Gajeong-ro, Daejeon 305-350, Republic of Korea

ABSTRACT The practical limits of coinage-metal-based plasmonic materials demand sustainable, abundant alternatives with a wide plasmonic range of the solar energy spectrum. Aluminum (Al) is an emerging alternative, but its instability in aqueous environments critically limits its applicability to various light-harvesting systems. Here, we report a design strategy to achieve a robust platform for plasmon-enhanced light harvesting using Al nanostructures. The incorporation of mussel-inspired polydopamine nanolayers in the Al nanoarrays allowed for the reliable use of Al plasmonic resonances in a highly corrosive photocatalytic redox solution and provided nanoscale arrangement of organic photosensitizers on Al surfaces. The Al—photosensitizer core—shell assemblies exhibited plasmon-enhanced light absorption, which resulted in a 300% efficiency increase in photo-to-chemical conversion. Our strategy enables stable and advanced use of aluminum for plasmonic light harvesting.



KEYWORDS: plasmon · aluminum · polydopamine · light harvesting · nanoantenna

Plasmon polaritons in metal nanostructures offer unusual optical capabilities to concentrate light into nanoscale volumes, supporting strong local field intensities.¹ This ability has attracted high interest in the field of energy harvesting for solar-to-electrical (or -chemical) energy conversion.^{2,3} Metal nanostructures that exhibit strong localized surface plasmon resonances (LSPR) in the visible spectrum have been adopted in various light-harvesting systems, such as solar cells and photocatalytic reactors, to transfer plasmonic energy to adjacent photosensitizers through resonant energy transfer or hot-electron injection.^{4–6} Considering the strong morphology and geometry dependence of LSPR that enable precise tailoring of optical properties for desirable light-harvesting systems,^{7,8} plasmonic metals would cause a breakthrough in efficiency improvements for solar energy conversion.

A number of reports demonstrated plasmon-enhanced light harvesting by utilizing well-known plasmonic materials

(*e.g.*, Au, Ag).^{9–11} However, their high costs and inherent limitations such as the limited spectral range of low-loss plasmonic resonances (>550 nm for Au and >400 nm for Ag) and the rapid oxidation of Ag degrading its plasmonic properties^{12–14} remain a hurdle. Recently, aluminum (Al) has been proposed as an alternative because it is cheap and covers up a wide spectrum range from UV to visible light of LSPR due to its high plasma frequency.^{15–19} Such properties are highly desirable for the practical realization of plasmon-enhanced solar energy applications. To date, however, only a few reports have demonstrated the utility of Al nanostructures in light-harvesting systems, and most of them were applied to solid-state platforms due to the poor stability of Al.^{20–23} While Al is stable in the atmosphere because of the protection by the formation of a surface oxide layer, its contact with an aqueous solution causes severe corrosion and limits the applicability of its unique plasmonic property. The passivation of Al surfaces using existing techniques may suppress such oxidation and corrosion

* Address correspondence to
ybshin@kribb.re.kr;
qubit@kaist.ac.kr;
parkcb@kaist.ac.kr.

Received for review March 11, 2015
and accepted June 5, 2015.

Published online June 05, 2015
10.1021/acsnano.5b01541

© 2015 American Chemical Society

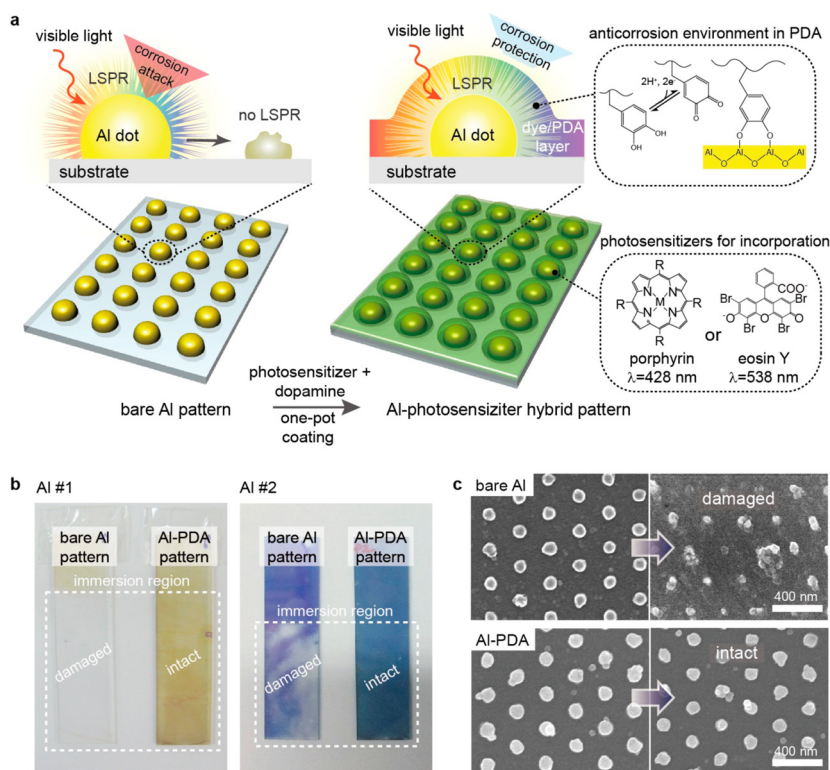


Figure 1. Stability of plasmonic Al nanoarrays. (a) Scheme of Al nanoarrays for plasmonic-enhanced light harvesting. The PDA coating enables precise incorporation of organic photosensitizers around the Al dots and provides an anticorrosion environment for the Al dots, allowing stable LSPR. (b, c) Stability of bare Al and Al-PDA patterns upon exposure to a photocatalytic redox solution for light harvesting ($10\ \mu\text{M}$ SnTPyP for Al #1 and $10\ \mu\text{M}$ eosin Y for Al #2 in TEOA–PB buffer), illustrated with (b) photographs and (c) SEM images.

problems, but this requires careful consideration of the spatial separation of light absorbers from LSPR regions of Al, which ultimately inhibits plasmonic enhancement in light harvesting.

Here, we present a new strategy for achieving robust and versatile light-harvesting platforms based on plasmonic Al nanostructures, as illustrated in Figure 1a. We created a nanoscale, conformal layer around the patterned Al dots through a simple polydopamine (PDA) coating, to protect the Al nanoarrays from corrosion and to accommodate organic photosensitizers in their LSPR regions. PDA is a mussel-inspired polymer that exhibits unique properties such as reductive capacity and universal applicability to any material.^{24,25} We demonstrate that the protective PDA shell with embedded photosensitizers can eliminate the critical problem of low spatial overlap between light absorbers and the LSPR field regions resulting from separate protection layers. The resulting corrosion-protected Al–photosensitizer hybrid patterns stably boosted photo-to-chemical conversion reactions in an aqueous solution due to plasmon-enhanced light absorption by the photosensitizers.

RESULTS AND DISCUSSION

We initiated our study by examining the stability of Al nanostructures and the protection effect of a PDA

coating against Al oxidation in an aqueous solution. We prepared two kinds of Al nanoarrays with different sizes and morphologies (Al #1: 111 nm in diameter and 60 nm in height; Al #2: 147 nm in diameter and 30 nm in height) through nanoimprint lithography, which exhibited distinctive optical properties (Figure S1, see the experimental section for details). For immersion corrosion tests, we adopted a photocatalytic redox solution as a model environment for light harvesting. The solution consisted of triethanolamine (TEOA) as an electron donor and organic photosensitizers, such as porphyrins and xanthene dyes, that can facilitate various photo-conversion reactions including nicotinamide cofactor (NAD^+) reduction.^{26,27} Among the porphyrin and xanthene derivatives, we selected Sn(IV) tetrakis(4-pyridyl) porphyrin (SnTPyP) and eosin Y (EY) as model photosensitizers. After overnight incubation in the redox solution, significant degradation of bare Al patterns was observed even with the naked eye, while PDA-coated Al patterns (Al-PDA) retained intact morphologies (Figure 1b). According to scanning electron microscopic analysis (Figures 1c and S2), many dots in the bare Al samples disappeared and the structures of the remaining dots could not be clearly discerned. In contrast, the nanostructures of Al-PDA did not show any noticeable changes after the incubation, which indicates a strong protective effect of PDA against the corrosion of Al.

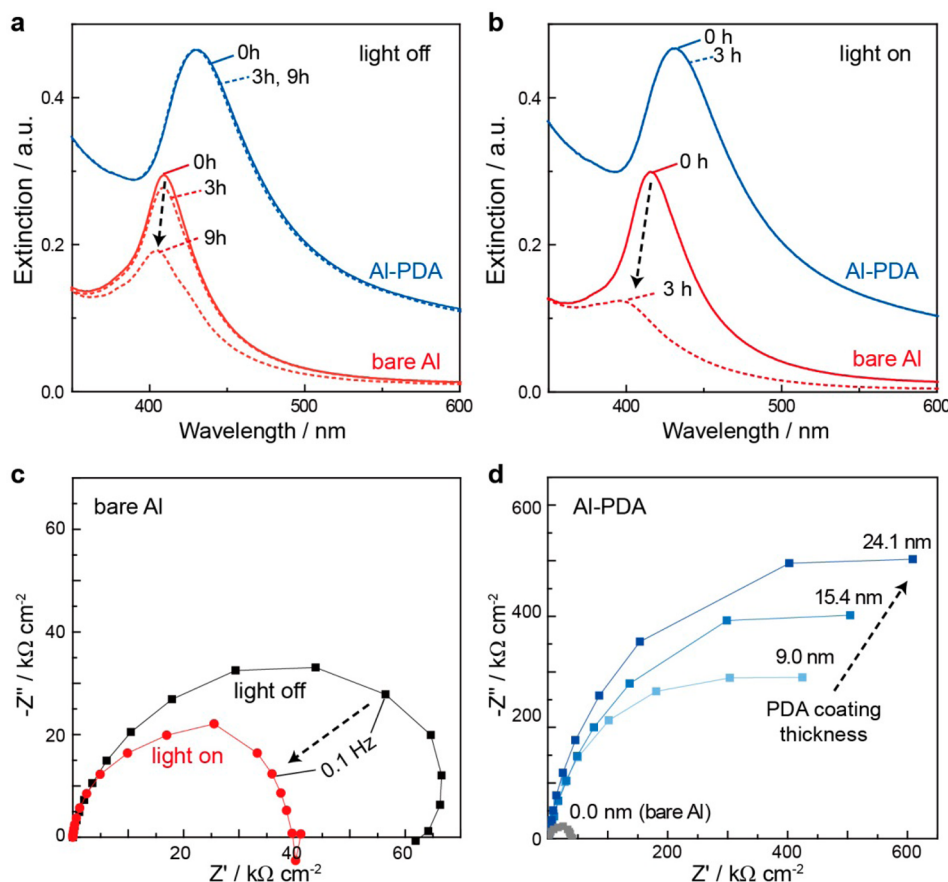


Figure 2. Corrosion behavior of Al nanoarrays. (a, b) Changes in plasmonic bands of Al #1 patterns incubated in a photocatalytic redox solution ($10 \mu\text{M}$ SnTPyP in TEOA–PB buffer) under (a) dark and (b) light conditions. (c) Nyquist plots of Al films with and without light irradiation after 2 h immersion in the photocatalytic redox solution. (d) Nyquist plots of Al films coated with PDA of different thicknesses after 2 h immersion in the photocatalytic redox solution under light irradiation.

Because spectral properties of plasmonic nanostructures are highly sensitive to their morphology changes,^{28,29} we investigated spectral changes in the plasmonic bands of Al nanoarrays upon exposure to the redox solution. The LSPR band for the bare Al nanoarrays gradually decreased and shifted toward shorter wavelengths (Figure 2a) because of the decrease in the particle sizes of Al dots. However, the Al-PDA showed no change either in the amplitude or in the position of its LSPR band under the same condition. The corrosion behavior of Al was strongly affected by the presence of light. Upon light illumination, the corrosion rate of the bare Al patterns was significantly accelerated (Figures 2b and S4). We used a 450 W Xe lamp ($\lambda > 420$ nm) as a light source. The light was incident normal to the surface of the sample on a glass substrate that was vertically immersed in the redox solution. Since the light exposure did not affect the corrosion of Al in the absence of photosensitizers (Figure S3), we attribute the accelerated corrosion to the light-induced redox reactions by the photosensitizers. The LSPR band of the PDA-coated Al pattern still remained stable under such corrosive conditions, which proved the applicability of Al-PDA plasmonic

nanostructures to solution-based light-harvesting applications. During prolonged incubation, the PDA coating exhibited a stable protection effect even after 2 weeks under both dark and light conditions (Figure S5).

To assess the corrosion resistance of Al and Al-PDA in the photocatalytic redox solutions, we performed electrochemical impedance spectroscopy (EIS) measurements. The EIS technique has been widely used to conduct electrochemical and kinetic studies on metal corrosion and to evaluate the performance of a protective coating on metal surfaces.³⁰ For the EIS measurements, we used Al films instead of Al nanoarrays because Al films allow a simpler circuit system compared to the nanoarrays. Note that nanoarrays should be formed on a conducting substrate (*e.g.*, ITO) for the EIS analysis, while Al films are conductive as is. To observe the light effect on the bare Al corrosion, we compared Nyquist plots of bare Al films after a 2 h immersion in the redox solution in the dark and light conditions, respectively (Figure 2c). Either the radius of semicircles or the impedance modulus at low frequency (*e.g.*, 0.1 Hz) in the Nyquist plots represents the degree of corrosion resistance originating from a sample surface; the bigger radius (or modulus) a

sample exhibits, the higher corrosion resistance it has.^{31–33} We found that the Al film under light irradiation was more easily eroded, which was consistent with the results analyzed by absorption spectroscopy in Figure 2b. We further investigated the protective effect of PDA against Al corrosion using EIS. Figure 2d shows Nyquist plots of Al films coated with PDA to different thicknesses, which were obtained after a 2 h immersion in the photocatalytic redox solution upon light irradiation. The PDA coating dramatically increased the corrosion resistance of Al and showed thickness dependence of the protective effect. During the immersion of Al in the redox solution, the conformal PDA layers would suppress direct contact of Al with corrosive electrolytes, and the chelation of surface Al atoms with catechol moieties^{34,35} can give additional passivation. On the basis of the spectroscopic results from immersion corrosion tests, we confirm that PDA protection allows reliable use of Al plasmonic resonances in the corrosive solutions during photocatalytic redox reactions.

We integrated photosensitizers into the protective PDA layer surrounding Al dots to achieve Al–photosensitizer core–shell assemblies for plasmonic resonance energy transfer. Considering the spectral match between plasmon resonance wavelength of the Al patterns and the absorption wavelength of the photosensitizers, we integrated Al #1 with SnTPyP (Al–SnTPyP) and Al #2 with EY (Al–EY) (Figure 3c,d). Through a simple immersion process of metal nanostructures in a solution containing both photosensitizer and dopamine molecules,³⁶ we produced elaborate core–shell assemblies, in which Al dots were surrounded by photosensitizer-encapsulating PDA shells in the nanoscale regime. From the increase in the diameters of Al dots after the photosensitizer-encapsulating PDA coating (Figures 3a,b and S6), we estimated the thicknesses of SnTPyP and EY shells to be approximately 10 to 12 nm using scanning electron microscopy and atomic force microscopy. We further confirmed the inclusion of photosensitizers in the PDA layers using XPS spectroscopy (Figure S7). The characteristic peaks of SnTPyP corresponding to Sn 3d_{3/2} and Sn 3d_{5/2} were observed at 497 and 477 eV, respectively, in the Al–SnTPyP assembly. The peaks of Br 3p at 190 eV and Br 3d at 69.5 eV indicate the inclusion of EY in the Al–EY assembly.

We investigated optical properties of the resulting nanohybrids by UV–vis absorption spectroscopy to observe plasmonic interactions between Al patterns and photosensitizers in the core–shell assembly. As shown in Figure 3c and d, the absorption bands of the photosensitizers at 427 nm (for SnTPyP) and 538 nm (for EY) were clearly identified in the Al–photosensitizer hybrid samples. We also observed spectral overlap between the absorption bands of the photosensitizers and the LSPR bands of the Al patterns. Note that the

plasmonic extinction has red-shifted after photosensitizer-encapsulating PDA coating due to the increased effective refractive index of the surrounding medium for Al dots. As a mutual result of the spectral overlap and the core–shell assembly, the hybrids exhibited enhanced intensity at the absorption band for the photosensitizers when compared to the spectrum of photosensitizer-encapsulating PDA films on bare glass substrates.

To better understand the nature of plasmon enhancement from Al patterns, we conducted finite-difference time-domain (FDTD) simulations for the Al–photosensitizer hybrid samples. As shown in Figure S8, the calculated results were consistent with the experimental results and confirmed that the plasmonic resonances of the Al patterns enhance the light absorptions of the photosensitizers. To examine the absorption contribution of each material region in the Al–photosensitizer hybrid system separately, we calculated the spatially resolved absorption spectra based on the spatial electric field profiles that were obtained from FDTD simulations (Figures 3e,f). Among the total absorption of the hybrid systems, the photosensitizer dominated the total absorption at the photosensitizer absorption region compared to the metal dots. The electric field profiles (Figures 3e,f, insets) indicate that strong local electric fields were induced over the photosensitizer-encapsulating PDA layers by Al plasmonic resonances, which result in plasmon-enhanced light absorption in the hybrid systems.

We further verified the LSPR effect of Al patterns in the Al–photosensitizer assemblies using surface-enhanced Raman scattering (SERS) measurements. When molecules locate in close proximity to the metal surfaces, they scatter more efficiently as they experience an enhanced electromagnetic field.^{37,38} We compared the Raman spectra of photosensitizer-encapsulating PDA films formed on Al patterns and bare glasses and observed a strong enhancement in the Raman signals of SnTPyP (Figure 4a) and EY (Figure S9a) on the Al patterns, which indicates plasmon-enhanced Raman scattering. We also measured photocurrent to see the plasmonic effect on photoinduced electron transfer. In a three-electrode system, we used Al–SnTPyP (or SnTPyP-encapsulating PDA) formed on an ITO glass as a working electrode and measured the photocurrent at an applied potential of -0.4 V (*vs* Ag/AgCl) during the on/off switching of visible light irradiation. As shown in Figure 4b, the net cathodic photocurrent of Al–SnTPyP was approximately 2.2 times higher than that of the SnTPyP-encapsulating PDA, which indicates that the Al nanostructures enabled the photosensitizer to convert light energy into electricity more effectively.

We applied Al–photosensitizer hybrid systems to biocatalytic artificial photosynthesis based on the high

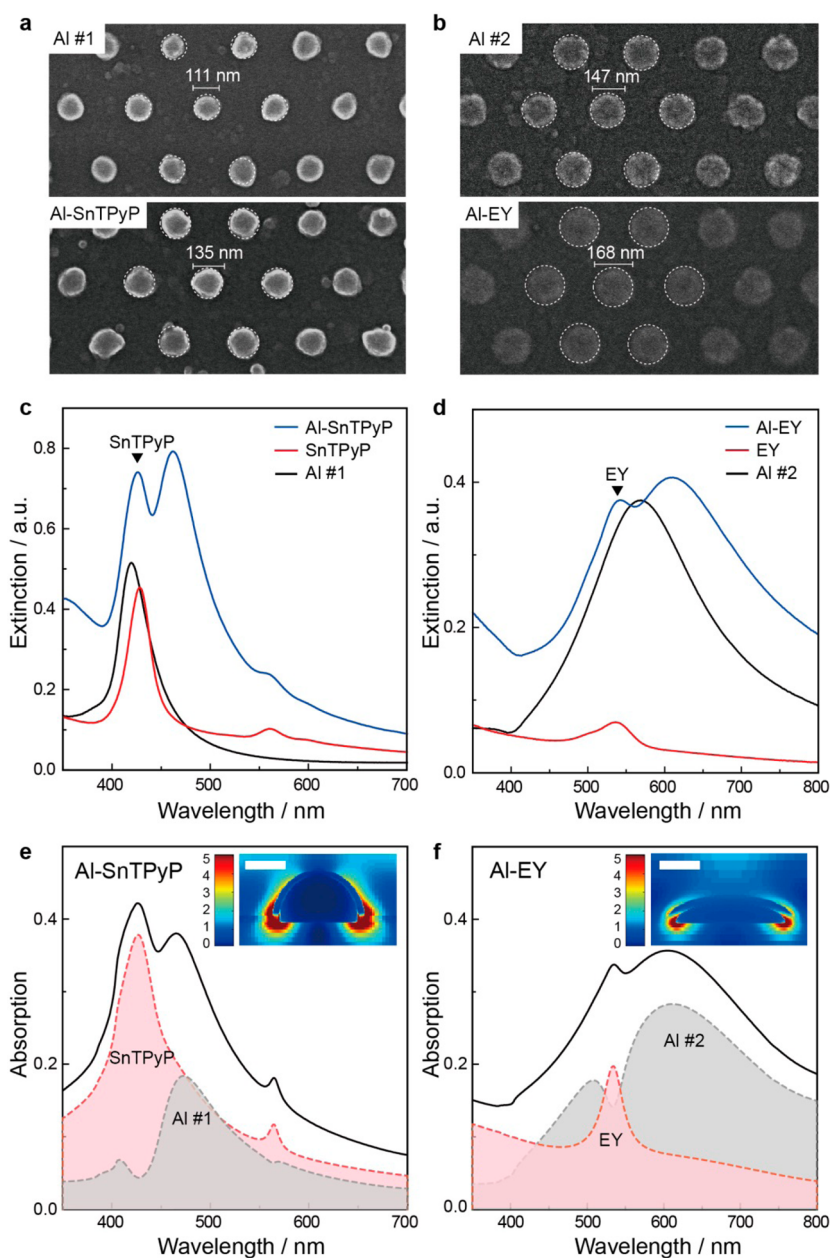


Figure 3. Morphologies and optical characterizations of Al nanoarrays. SEM images of (a) Al #1 before and after hybridization with SnTPyP-encapsulating PDA and (b) Al #2 before and after hybridization with EY-encapsulating PDA. Extinction spectra of (c) pristine Al #1, SnTPyP-encapsulating PDA on bare glass, Al-SnTPyP hybrid, (d) pristine Al #2, EY-encapsulating PDA on bare glass, and Al-EY hybrid. (e, f) Simulated absorption of Al–photosensitizer hybrids. The total absorption (solid lines) as well as individual absorption contribution from each material region (dashed lines) are plotted. The insets illustrate electric field enhancement plots of the Al dots surrounded by photosensitizer-encapsulating PDA shells (10 nm). The scale bar corresponds to 50 nm.

stability and effectivity of LSPR from the PDA-coated Al patterns. As a model light-harvesting system mimicking natural photosynthesis in green plants,^{39–41} we conducted a light-induced reduction of nicotinamide cofactor (NAD^+) using the Al–photosensitizer core–shell assemblies. During the photoconversion, the photosensitizer facilitates visible-light-induced reduction of NAD^+ to NADH, which functions as an electron-donating cofactor for various NADH-dependent redox enzymes to produce valuable chemicals (Figure 4c). As shown in Figure 4d, the inclusion of Al markedly

increased the NADH conversion yield by SnTPyP from $5.3 \mu\text{M}$ to $12.5 \mu\text{M}$ after a 3 h photocatalytic reaction, which indicates plasmon-derived light-harvesting enhancement. The Al-EY hybrid also exhibited a higher NADH conversion yield compared to the EY-encapsulating PDA film (Figure S8b). Note that bare Al patterns exhibited no catalytic effect on NADH conversion. We evaluated plasmon enhancement factors for light harvesting, considering the difference in the surface area between the Al-patterned substrate and the bare glass substrate to better match the degree of

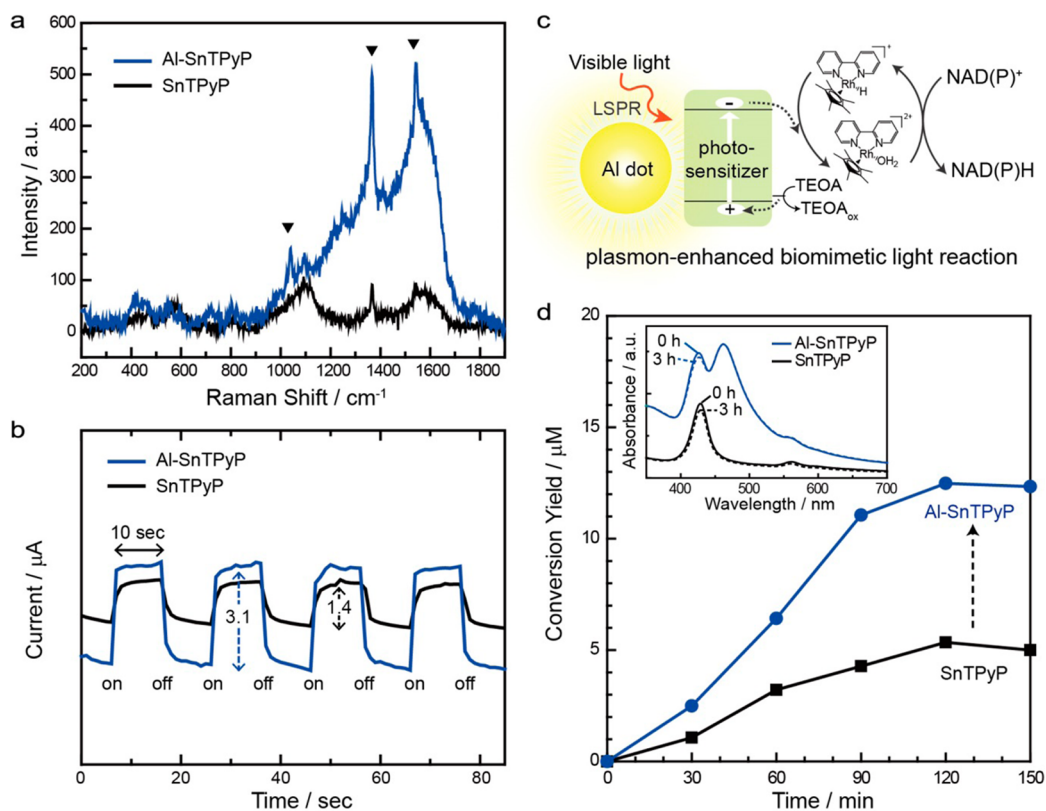


Figure 4. Plasmonic enhancements by Al nanoarrays. (a) Comparison of the SERS spectra for the SnTPyP-encapsulating PDA film and Al-SnTPyP hybrid. (b) Photocurrent responses of the SnTPyP-encapsulating PDA film and Al-SnTPyP hybrid formed on ITO glasses during visible-light on/off switching. (c) Illustrative scheme of biomimetic NADH photoregeneration using plasmon-enhanced light-harvesting systems. (d) Comparison of the NADH photoregeneration yield using a SnTPyP-encapsulating PDA film Al-SnTPyP hybrid under visible light irradiation. The inset shows the absorbance spectra of the SnTPyP-encapsulating PDA film and Al-SnTPyP hybrid before and after the photocatalytic reaction for 3 h, indicating the high stability of Al LSPR.

photosensitizer coverage. For the Al-patterned substrate, one side of the substrate had a surface area increase of a factor of 1.4 due to the nonplanar Al patterns, while the other side, devoid of Al, had the same area as the bare glass substrate. Note that the photosensitizer-encapsulating PDA film covered both sides of the substrates due to the immersion process. As a result, the plasmon enhancement factors were calculated to be 2.6 and 3.0 for Al-SnTPyP and Al-EY, respectively. We further compared the photocatalytic efficiencies of SnTPyP in the PDA layers formed on plasmonic and nonplasmonic nanoarrays, respectively. The nonplasmonic nanoarrays (Al500) were prepared by heat treatment of plasmonic Al nanoarrays in the air condition at 500 °C (Figure S10a). As expected, the Al-SnTPyP hybrid exhibited a much higher conversion yield compared to the nonplasmonic Al500-SnTPyP hybrid, which confirms the effect of plasmon resonance energy transfer from Al nanoarrays (Figure S10b). We expect that much room exists for further improvements in plasmonic enhancement by achieving an ideal spectral overlap and optimal densities of photosensitizers and Al dots. On the basis of the negligible changes in the optical properties for the Al-SnTPyP sample after the light-harvesting reaction (Figure 4d,

inset), we further confirmed the high stability of our plasmonic light-harvesting assemblies against corrosion.

CONCLUSION

We achieved a reliable light-harvesting platform based on Al nanostructures that can be stably utilized in an aqueous environment to facilitate plasmon-enhanced solar-to-chemical energy conversion. We successfully prevented the accelerated corrosion of the Al nanostructures in photocatalytic environments by PDA protection to preserve Al plasmonic resonances. We then developed elaborate core-shell assemblies, in which photosensitizers were encapsulated in the LSPR regions of Al dots by simultaneous coating with PDA for plasmon-enhanced light absorption. The resulting Al-photosensitizer assemblies exhibited plasmonic enhancements in the visible-light-induced photocurrent generation and biomimetic photo-chemical conversion, while showing high stability in optical and physical properties against corrosion in the photocatalytic redox solution. This approach of combining Al patterns and photosensitizers in core-shell nanostructures enables various designs of plasmon-enhanced light-harvesting platforms with tailorable and stable optical properties.

Conflict of Interest: The authors declare no competing financial interest.

Supporting Information Available: Experimental details, additional characterizations of Al nanoarrays, corrosion behavior of Al arrays, simulated absorbance spectra of Al–photosensitizer hybrids, plasmonic enhancement results from Al-EY, and schematic illustration of Al nanoarray synthesis. The Supporting Information is available free of charge on the ACS Publications website at DOI: 10.1021/acsnano.5b01541.

Acknowledgment. This study was supported by grants from the National Research Foundation (NRF) via the National Leading Research Laboratory (NRF-2013R1A2A1A05005468) and the Intelligent Synthetic Biology Center of Global Frontier R&D Project (2011-0031957), Republic of Korea. This work was supported in part by the National Research Foundation of Korea (NRF) grant funded by the Korea government (MSIP) (NRF-2013M3C1A3063598).

REFERENCES AND NOTES

- Barnes, W. L.; Dereux, A.; Ebbesen, T. W. Surface Plasmon Subwavelength Optics. *Nature* **2003**, *424*, 824–830.
- Linic, S.; Christopher, P.; Ingram, D. B. Plasmonic-Metal Nanostructures for Efficient Conversion of Solar to Chemical Energy. *Nat. Mater.* **2011**, *10*, 911–921.
- Atwater, H. A.; Polman, A. Plasmonics for Improved Photovoltaic Devices. *Nat. Mater.* **2010**, *9*, 205–213.
- Ferry, V. E.; Munday, J. N.; Atwater, H. A. Design Considerations for Plasmonic Photovoltaics. *Adv. Mater.* **2010**, *22*, 4794–4808.
- Warren, S. C.; Thimsen, E. Plasmonic Solar Water Splitting. *Energy Environ. Sci.* **2012**, *5*, 5133–5146.
- Clavero, C. Plasmon-Induced Hot-Electron Generation at Nanoparticle/Metal-Oxide Interfaces for Photovoltaic and Photocatalytic Devices. *Nat. Photonics* **2014**, *8*, 95–103.
- Tan, S. J.; Campolongo, M. J.; Luo, D.; Cheng, W. Building Plasmonic Nanostructures with DNA. *Nat. Nanotechnol.* **2011**, *6*, 268–276.
- Hou, S.; Hu, X.; Wen, T.; Liu, W.; Wu, X. Core–Shell Noble Metal Nanostructures Templated by Gold Nanorods. *Adv. Mater.* **2013**, *25*, 3857–3862.
- Hou, W.; Cronin, S. B. A Review of Surface Plasmon Resonance-Enhanced Photocatalysis. *Adv. Funct. Mater.* **2013**, *23*, 1612–1619.
- Mori, K.; Kawashima, M.; Che, M.; Yamashita, H. Enhancement of the Photoinduced Oxidation Activity of a Ruthenium(II) Complex Anchored on Silica-Coated Silver Nanoparticles by Localized Surface Plasmon Resonance. *Angew. Chem., Int. Ed.* **2010**, *49*, 8598–8601.
- Mubeen, S.; Lee, J.; Singh, N.; Kramer, S.; Stucky, G. D.; Moskovits, M. An Autonomous Photosynthetic Device in Which All Charge Carriers Derive from Surface Plasmons. *Nat. Nanotechnol.* **2013**, *8*, 247–251.
- Naik, G. V.; Shalae, V. M.; Boltasseva, A. Alternative Plasmonic Materials: Beyond Gold and Silver. *Adv. Mater.* **2013**, *25*, 3264–3294.
- Sachan, R.; Ramos, V.; Malasi, A.; Yadavali, S.; Bartley, B.; Garcia, H.; Duscher, G.; Kalyanaraman, R. Oxidation-Resistant Silver Nanostructures for Ultrastable Plasmonic Applications. *Adv. Mater.* **2013**, *25*, 2045–2050.
- Lal, S.; Link, S.; Halas, N. J. Nano-Optics from Sensing to Waveguiding. *Nat. Photonics* **2007**, *1*, 641–648.
- Langhammer, C.; Schwind, M.; Kasemo, B.; Zorić, I. Localized Surface Plasmon Resonances in Aluminum Nanodisks. *Nano Lett.* **2008**, *8*, 1461–1471.
- Bisio, F.; Proietti Zaccaria, R.; Moroni, R.; Maidecchi, G.; Alabastri, A.; Gonella, G.; Giglia, A.; Andolfi, L.; Nannarone, S.; Mattera, L.; *et al.* Pushing the High-Energy Limit of Plasmonics ACS Nano DOI: 10.1021/nn503035b.
- Knight, M. W.; King, N. S.; Liu, L.; Everitt, H. O.; Nordlander, P.; Halas, N. J. Aluminum for Plasmonics. *ACS Nano* **2014**, *8*, 834–840.
- Knight, M. W.; Liu, L.; Wang, Y.; Brown, L.; Mukherjee, S.; King, N. S.; Everitt, H. O.; Nordlander, P.; Halas, N. J. Aluminum Plasmonic Nanoantennas. *Nano Lett.* **2012**, *12*, 6000–6004.
- Schwab, P. M.; Moosmann, C.; Wissert, M. D.; Schmidt, E. W. G.; Ilin, K. S.; Siegel, M.; Lemmer, U.; Eisler, H.-J. Linear and Nonlinear Optical Characterization of Aluminum Nanoantennas. *Nano Lett.* **2013**, *13*, 1535–1540.
- Zheng, B. Y.; Wang, Y.; Nordlander, P.; Halas, N. J. Color-Selective and CMOS-Compatible Photodetection Based on Aluminum Plasmonics. *Adv. Mater.* **2014**, *26*, 6318–6323.
- Villesen, T. F.; Uhrenfeldt, C.; Johansen, B.; Larsen, A. N. Self-Assembled Al Nanoparticles on Si and Fused Silica, and Their Application for Si Solar Cells. *Nanotechnology* **2013**, *24*, 275606.
- Kakavelakis, G.; Stratakis, E.; Kymakis, E. Aluminum Nanoparticles for Efficient and Stable Organic Photovoltaics. *RSC Adv.* **2013**, *3*, 16288–16291.
- Hylton, N. P.; Li, X. F.; Giannini, V.; Lee, K. H.; Ekins-Daukes, N. J.; Loo, J.; Verduyck, D.; Van Dorpe, P.; Sodabanlu, H.; Sugiyama, M., *et al.* Loss Mitigation in Plasmonic Solar Cells: Aluminium Nanoparticles for Broadband Photocurrent Enhancements in GaAs Photodiodes. *Sci. Rep.* **2013**, *3*, 2874.
- Lee, H.; Dellatore, S. M.; Miller, W. M.; Messersmith, P. B. Mussel-Inspired Surface Chemistry for Multifunctional Coatings. *Science* **2007**, *318*, 426–430.
- Ryu, J.; Ku, S. H.; Lee, H.; Park, C. B. Mussel-Inspired Polydopamine Coating as a Universal Route to Hydroxyapatite Crystallization. *Adv. Funct. Mater.* **2010**, *20*, 2132–2139.
- Lee, S. H.; Nam, D. H.; Kim, J. H.; Baeg, J.-O.; Park, C. B. Eosin Y-Sensitized Artificial Photosynthesis by Highly Efficient Visible-Light-Driven Regeneration of Nicotinamide Cofactor. *ChemBioChem* **2009**, *10*, 1621–1624.
- Oppelt, K. T.; Wöß, E.; Stiftinger, M.; Schöffberger, W.; Buchberger, W.; Knör, G. Photocatalytic Reduction of Artificial and Natural Nucleotide Co-factors with a Chlorophyll-Like Tin-Dihydroporphyrin Sensitizer. *Inorg. Chem.* **2013**, *52*, 11910–11922.
- Baraldi, G.; Carrada, M.; Toudert, J.; Ferrer, F. J.; Arbouet, A.; Paillard, V.; Gonzalo, J. Preventing the Degradation of Ag Nanoparticles Using an Ultrathin α -Al₂O₃ Layer as Protective Barrier. *J. Phys. Chem. C* **2013**, *117*, 9431–9439.
- Reed, J. C.; Zhu, H.; Zhu, A. Y.; Li, C.; Cubukcu, E. Graphene-Enabled Silver Nanoantenna Sensors. *Nano Lett.* **2012**, *12*, 4090–4094.
- Bierwagen, G.; Tallman, D.; Li, J.; He, L.; Jeffcoate, C. EIS Studies of Coated Metals in Accelerated Exposure. *Prog. Org. Coat.* **2003**, *46*, 149–158.
- Haase, M. F.; Grigoriev, D. O.; Möhwald, H.; Shchukin, D. G. Development of Nanoparticle Stabilized Polymer Nanocontainers with High Content of the Encapsulated Active Agent and Their Application in Water-Borne Anticorrosive Coatings. *Adv. Mater.* **2012**, *24*, 2429–2435.
- Shchukin, D. G.; Zheludkevich, M.; Yasakau, K.; Lamaka, S.; Ferreira, M. G. S.; Möhwald, H. Layer-by-Layer Assembled Nanocontainers for Self-Healing Corrosion Protection. *Adv. Mater.* **2006**, *18*, 1672–1678.
- Hollamby, M. J.; Borisova, D.; Mohwald, H.; Shchukin, D. Porous 'Ouzo-Effect' Silica-Ceria Composite Colloids and Their Application to Aluminium Corrosion Protection. *Chem. Commun.* **2012**, *48*, 115–117.
- Cornard, J. P.; Lapouge, C. Theoretical and Spectroscopic Investigations of a Complex of Al(III) with Caffeic Acid. *J. Phys. Chem. A* **2004**, *108*, 4470–4478.
- Tulevski, G. S.; Miao, Q.; Fukuto, M.; Abram, R.; Ocko, B.; Pindak, R.; Steigerwald, M. L.; Kagan, C. R.; Nuckolls, C. Attaching Organic Semiconductors to Gate Oxides: *In Situ* Assembly of Monolayer Field Effect Transistors. *J. Am. Chem. Soc.* **2004**, *126*, 15048–15050.
- Lee, M.; Kim, J. U.; Lee, J. S.; Lee, B. I.; Shin, J.; Park, C. B. Mussel-Inspired Plasmonic Nanohybrids for Light Harvesting. *Adv. Mater.* **2014**, *26*, 4463–4468.

37. Mogensen, K. B.; Guhlke, M.; Kneipp, J.; Kadkhodazadeh, S.; Wagner, J. B.; Espina Palanco, M.; Kneipp, H.; Kneipp, K. Surface-Enhanced Raman Scattering on Aluminum Using Near Infrared and Visible Excitation. *Chem. Commun.* **2014**, *50*, 3744–3746.
38. Jha, S. K.; Ahmed, Z.; Agio, M.; Ekinci, Y.; Löffler, J. F. Deep-UV Surface-Enhanced Resonance Raman Scattering of Adenine on Aluminum Nanoparticle Arrays. *J. Am. Chem. Soc.* **2012**, *134*, 1966–1969.
39. Kim, J. H.; Nam, D. H.; Park, C. B. Nanobiocatalytic Assemblies for Artificial Photosynthesis. *Curr. Opin. Biotechnol.* **2014**, *28*, 1–9.
40. Liu, J.; Antonietti, M. Bio-Inspired NADH Regeneration by Carbon Nitride Photocatalysis Using Diatom Templates. *Energy Environ. Sci.* **2013**, *6*, 1486–1493.
41. Oppelt, K. T.; Gasiorowski, J.; Egbe, D. A. M.; Kollender, J. P.; Himmelsbach, M.; Hassel, A. W.; Sariciftci, N. S.; Knör, G. A Rhodium Coordinated Poly(arylene-ethynylene)-alt-poly(arylene-vinylene) Copolymer Acting as Photocatalyst for Visible-Light Powered NAD^+ /NADH Reduction. *J. Am. Chem. Soc.* **2014**, *136*, 12721–12729.